Au/PS-coated hollow fibers without dielectric absorption. The transmission wavelength is taken as 200 μm. It can be seen in Fig.3 that the losses in the three cases all decrease as the inner diameter increases. The additional losses introduced by dielectric absorption can be easily observed when comparing the two curves corresponding to Au/PS hollow fiber. When the inner diameter is smaller than 0.87 mm, Au/PS hollow fiber with dielectric absorption has higher transmission losses than the Au-coated hollow fiber. That is, for the transmission of 200 μm THz wave, the inner diameter of an Au/PS-coated hollow fiber should be greater than 0.87 mm in order to obtain lower transmission loss than an Au-coated hollow fiber of the same bore size. When the inner diameter is smaller than 0.46 mm, the loss of the Au/PS-coated hollow fiber is higher than that of the Au-coated ones even with a perfect transparent PS layer. It is almost impossible to lower the loss by a dielectric inner-coating (n = 1.5) at the wavelength of 200 μm for the small-bore metallic hollow fiber.

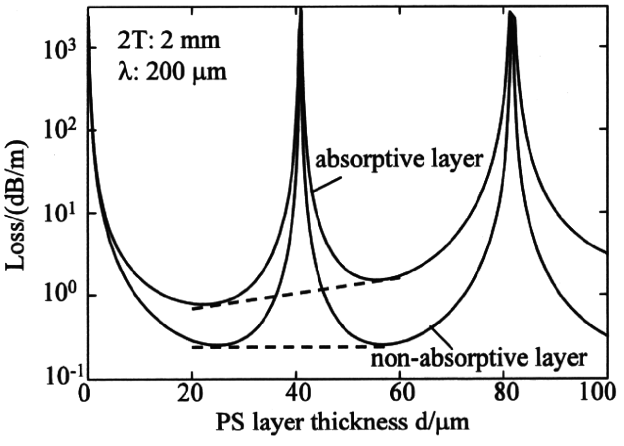

Figure 2: Transmission losses of the HE_{11} mode as a function of PS layer thickness

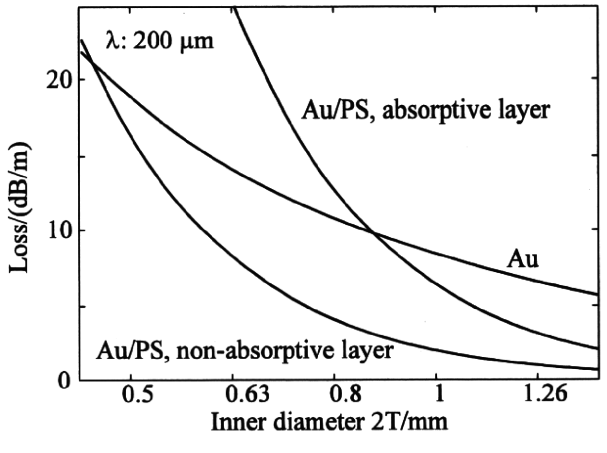

Figure 3: Transmission loss of THz hollow fiber as a function of inner diameter

Then, the influences of dielectric absorption on the optimum dielectric refractive index are investigated. The parameter of F_d in Equation (8) and the losses of HE_{11} modes with the variation of dielectric refractive index are shown in Fig. 4. In the calculation, the absorption coefficient of the absorptive dielectric layer is 2.4 cm^{-1}, the wavelength is 200 μm and inner diameter is 2 mm. It had been shown that the optimum dielectric refractive index that minimizes the loss of HE_{11} mode is 1.41 in the absence of dielectric absorption [9], which is also shown in Fig. 4. It is observed that the parameter F_d, which is proportional to absorption loss $\Delta\alpha$ as indicated in Equation (8), decreases with the increase of n_d. Consequently, when dielectric absorption is taken into consideration, the optimum dielectric refractive index turns out to be greater than 1.41. The value depends on such factors as inner diameter, transmission wavelength and refractive index of the metal layer. In the case of Fig. 4, the optimum dielectric refractive index is 2.1. In the area of $n_d < 1.5$, the loss of HE_{11} mode considering dielectric absorption rises rapidly with the decrease of n_d. This is due to the impact of the parameter of F_d. So when the dielectric absorption is taken into consideration, dielectric material with low refractive index is not a good choice.

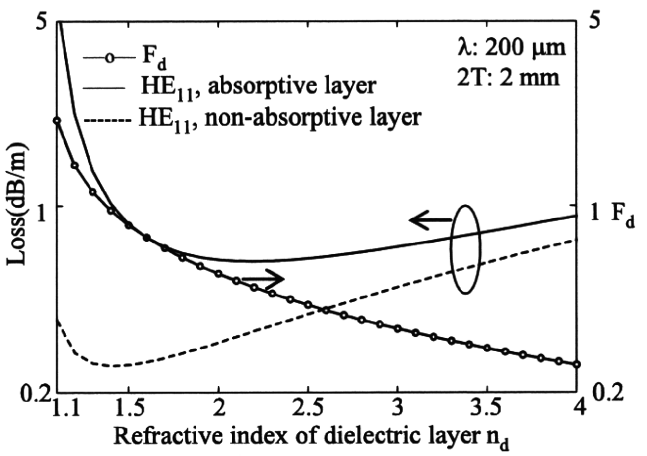

Figure 4: F_d and losses of HE_{11} mode as a function of n_d

Lastly, absorption tolerance is analyzed. Absorption tolerance is defined as the absorption coefficient when the loss of dielectric-coated metallic hollow fiber is equal to that of metallic hollow fiber of the same bore size. To design a low-loss dielectric-coated metallic hollow fiber, it is necessary to know the absorption tolerance in advance. It depends on such factors as inner diameter, transmission wavelength, the refractive index of the dielectric layer and the metal layer. Here, the metal layer is assumed to be Au.

The relationship between the absorption tolerance and the inner diameter is shown in Fig. 5. Calculations were made for dielectric layers of different refractive index. The transmission wavelength is 200 μm. It is observed that the tolerance increases as the bore size becomes larger. Compared with other curves, Curve 4 has much lower absorption tolerance. In the case of Curve 4, the absorption tolerance is as low as 1 cm^{-1} even when the inner diameter reaches 2 mm. It indicates that the dielectric material with n_d=1.1 is not a suitable one for the hollow fiber. Note that Curve 1 and Curve 2 have no numerical values in the area of

2T<0.68 mm and 2T<0.52 mm respectively. That is because even the perfect transparent dielectric layer can no longer lower the loss of a metallic hollow fiber when the inner diameter is small. In that case, the absorption tolerance does not exist. A special case of this phenomenon has be shown in Fig. 3 where the loss of Au/PS hollow with non-absorptive PS layer is higher than that of Au hollow fiber when the inner diameter is less than 0.46 mm. It indicates that the refractive index of the dielectric layer should be carefully selected for the THz hollow fiber of small bore size. In the case of Fig. 5, only the dielectric material with $n_d = 1.5$ is usable when the inner diameter is 0.5 mm.

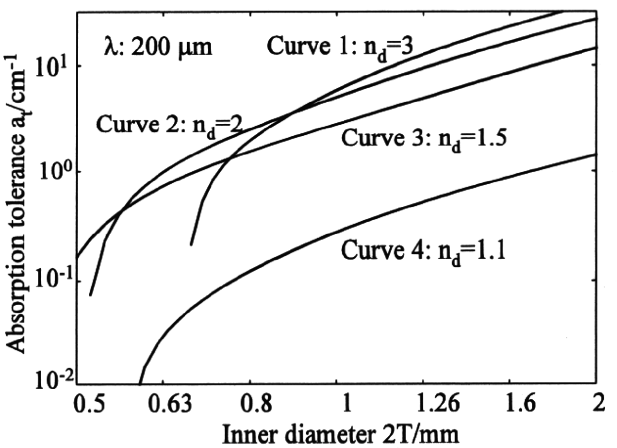

Figure 5: Absorption tolerance of fibers with different inner diameters

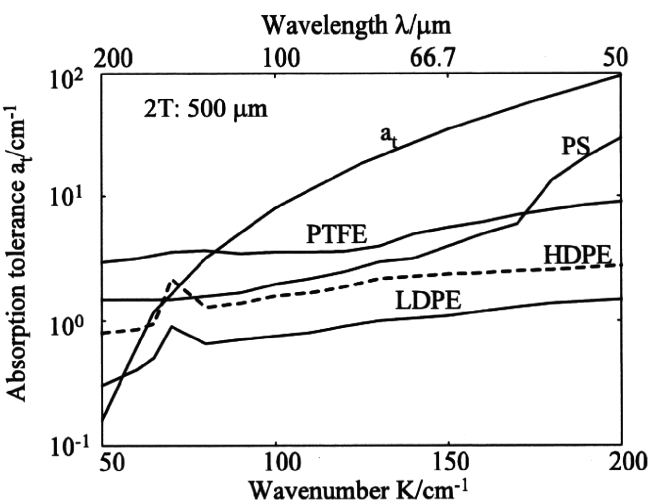

Figure 6: Absorption tolerance and absorption spectra of polymers

The absorption tolerance as a function of wave number is shown in Fig. 6. Absorption properties of four dielectric materials, Polytetrafluoroethylene (PTFE), Polystyrene (PS), High Density Polyethylene (HDPE) and Low Density Polyethylene (LDPE) [12, 13], are also added for comparison. n_d is 1.5 for the calculation

because the refractive indices of the four materials are all around 1.5 at the THz region. It is observed in Fig. 6 that the tolerance increases with the increase of the wave number. From wave number 50 cm^{-1} to 200 cm^{-1}, the absorption tolerance increases by more than two orders of magnitude. When the transmission wave number is greater than 100 cm^{-1}, all of the four materials are acceptable. Whereas, none of these materials is usable when the wave number is 50 cm^{-1}. As shown in Fig. 6, LDFE has low absorption in the THz region and is one of the best choices as dielectric layer materials.

It is worth mentioning that in some cases the absorption tolerance does not exist. One of such cases, which had been shown in Fig.3 and Fig.5, is that the inner diameter of the hollow fiber is small. Another case is that the transmission wavelength is long. This is because with the increase of the transmission wavelength, the transmission losses of TE_{11} mode for metallic hollow fibers decrease while the transmission losses of HE_{11} mode for dielectric-coated metallic hollow fibers increase.

5. Conclusions

The influences of dielectric absorption on the structure parameters of dielectric-coated metallic hollow fibers including optimum dielectric layer thickness, the optimum dielectric refractive index and the inner diameter are studied. When dielectric absorption is taken into consideration, the optimum dielectric layer thickness becomes smaller and optimum dielectric refractive index becomes larger. For hollow fiber with small bore size, the refractive index of the dielectric layer should be carefully selected.

The absorption tolerance is also investigated considering the factors of inner diameter, the refractive index, and the operating wavelength. The absorption tolerance decreases as the inner diameter becomes smaller or the transmission wavelength becomes larger. In extreme cases of small inner-diameter or large transmission wavelength, the absorption tolerance does not exist.

6. Acknowledgements

This work is financially supported by the Shanghai Pujiang program (7pj14012) and the Ministry of Education, Science, Sports and Culture of Japan through Grant-in-Aids for Scientific Research (B) (20360164).

References

1. K. Wang and D. M. Mittleman, "Metal wires for terahertz wave guiding," Nature, **432,** 376-379 (2004).
2. T. Ito, Y. Matsuura, M. Miyagi, H. Minamide, and H. Ito, "Flexible terahertz fiber optics with low bend-induced losses," J. Opt. Soc. Am. B, **24,** 1230-1235 (2007).
3. R. Mendis and D. Grischkowsky, "Plastic ribbon THz waveguides," J. Appl. Phys., **88,** 4449-4451 (2000).
4. H. Han, H. Park, M. Cho, and J. Kim, "Terahertz pulse propagation in a plastic photonic crystal," Appl. Phys. Lett., **80,** 2634-2636 (2002).

5. M. Skorobogatiy and A. Dupuis, "Ferroelectric all-polymer hollow Bragg fibers for terahertz guidance," Appl. Phys. Lett. **90,** 113514 (2007).
6. L. J. Chen, H. W. Chen, T. F. Kao, J. Y. Lu, and C. K. Sun, "Low-loss subwavelength plastic fiber for terahertz waveguiding," Opt. Lett., **31,** 308-310 (2006).
7. B. Bowden, J. A. Harrington, and O. Mitrofanov. "Silver/polystyrene-coated hollow glass waveguides for the transmission of terahertz radiation," Opt. Lett., **32,** 2945-2947 (2007).
8. Y. W. Shi, K. Ito, L. Ma, T. Yoshida, Y. Matsuura, and M. Miyagi, "Fabrication of a polymer-coated silver hollow optical fiber with high performance," Appl. Opt., **45,** 6736-3670 (2006).
9. M. Miyagi and S. Kawakami, "Design theory of dielectric coated circular metallic waveguides for infrared Transmission," J. Lightw. Technol. **LT-2,** 116-126 (1984).
10. C. Themistos, B. M. A. Rahman, M. Rajarajan, K. T. V. Grattan, B. Bowden, and J. A. Harrington, "Characterization of Silver/Polystyrene (PS)-coated hollow glass waveguides at THz frequency," J. Lightw. Technol. **LT-2,** 2456-2462 (2007).
11. R. K. Nubling and J. A. Harrington, "Launch conditions and mode coupling in hollow-glass waveguides," Opt. Eng., **37,** 2454-2458 (1998).
12. J. R. Birch, "The far-infrared optical constants of polypropylene, PTFE and polystyrene," Infrared Phys. **33,** 33-38 (1992).
13. J. R. Birch, "The far infrared optical constants of polyethylene," Infrared Phys. **30,** 195-197 (1990).

Fabrication of SiO_2/AgI/SiO_2/Ag Hollow Glass Fiber for Infrared Transmission

Ke-Rong Sui[1], Xiao Lin[1], Xiao-Song Zhu[1], Yi-Wei Shi[1], Katsumasa Iwai[2], and Mitsunobu Miyagi[2, 3]

1. Department of Communication Science and Engineering, Fudan University, Shanghai 200433, China. Email: ywshi@fudan.edu.cn
2. Sendai National College of Technology, Sendai, 989-3128, Japan
3. Miyagi National College of Technology, Sendai, 981-1239, Japan

Abstract

Transmission characteristics of infrared hollow fiber with multi- AgI and SiO_2 films are discussed. Three-dielectric-layer hollow glass fiber with SiO_2/AgI/SiO_2/Ag structure was fabricated for low-loss delivery of infrared laser light. The first SiO_2 film on the silver layer was coated by using liquid phase coating method. A semi-inorganic polymer was used as the coating material. A smooth vitreous film was formed by the treatment of a hardener at room temperature and followed by curing treatment. For the deposition of the AgI film between the two SiO_2 films, an Ag film was first plated on the SiO_2 film by silver mirror reaction method. Then the iodination process was conducted to turn the silver layer into silver iodide. The second SiO_2 layer was deposited on the AgI layer in the same way as the first SiO_2 layer. Fabrication parameters for controlling film thicknesses, such as iodination temperature, silver mirror reaction time, and solution concentration, are clarified for depositing AgI and SiO_2 films with the theoretical optimum thicknesses. By optimizing the thickness of the three dielectric layers, low-loss in the loss spectrum of SiO_2/AgI/SiO_2/Ag hollow glass waveguides can be obtained at the target infrared wavelengths. A method is proposed to evaluate the film thickness of AgI layer based on the positions of loss peaks and valleys in the loss spectra. Theoretical calculation for loss spectrum of SiO_2/AgI/SiO_2/Ag hollow glass fiber considering material dispersion of dielectric materials is also conducted. Good agreement with the measured data is demonstrated.

Key words: hollow fiber, infrared, multi-layer, silicone polymer, silver iodide, material dispersion

1. Introduction

Hollow fiber is one of the most commonly used infrared transmission media [1-4] for delivering infrared laser light in recently years. The hollow fiber inner-coated with metal layer and dielectric layer has low transmission loss in the infrared regions. It is capable of delivering various kinds of useful infrared lasers widely used in medical and industry fields, including Nd:YAG, Ho:YAG, Er:YAG, CO, and CO_2 lasers. The low-loss property of this kind of fiber can be attained at a target wavelength by selecting an appropriate dielectric film thickness according to the design theory [5]. Besides optimizing the dielectric film thickness, increasing the number of dielectric layers is also an effective method to lower the attenuation of the hollow fiber. Hence multiple dielectric layer hollow fiber has been one of the hottest researches in the hollow fiber field.

The structure composed of periodically depositing dielectric layers of low and high refractive indexes [6-7], is one of the most commonly used structures for multiple dielectric layer hollow fibers. Theoretically, multilayered structure will contribute to the decrease of transmission loss for delivering

Optical Fibers and Sensors for Medical Diagnostics and Treatment Applications IX, edited by Israel Gannot, Proc. of SPIE Vol. 7173, 71730G · © 2009 SPIE · CCC code: 1605-7422/09/$18 · doi: 10.1117/12.807904

infrared lasers, whereas there are several obstacles in developing multilayered hollow fiber. One difficulty is the fabrication technique for a uniform and durable hollow fiber. The glass-drawing technique [8] used for fabricating optical fiber is not easy to apply to the fabrication of multilayered hollow fiber. It is difficult to find two materials which can maintain the origin structure after the co-draw process. Because these two materials have different characteristics when proceed in the glass-drawing technique. Other fabrication methods involving sputtering, electroplating coating [9], chemical vapor deposition (CVD) [10], and liquid phase chemistry method [11] are proposed. However it is still not easy to fabricate the hollow fiber of multiple layers. Secondly, due to the existence of non-uniformity of inner coated dielectric film surfaces, the additional loss generated by surface roughness will accumulated with the increase of layer number. Besides, the selection for dielectric film remains a dilemma. Two dielectric materials used in the low/high stacking structure need to have good adhesion to make a durable hollow fiber. In this circumstance, these two materials tend to have similar optical property, while high refractive index contrast against each other for these two materials is necessary for low-loss hollow fiber. Despite all these complexity and hardness, the low loss property is attractive in this research field. Recently, several different multilayer designs, such as the multiple-layer hollow fiber using PbS and CdS [12], Ta_2O_5 and SiO_2 [13] were proposed and fabricated.

In this paper, we fabricated a three dielectric-layer structure hollow fiber. We choose AgI and SiO_2 as the dielectric materials. The hollow fiber with the structure of SiO_2/AgI/SiO_2/Ag was fabricated for low-loss delivery of infrared laser. We have carried out researches and some good experimental results were obtained when using these two materials separately [14-15]. The SiO_2/AgI/SiO_2/Ag structure for hollow fiber has several advantages. These two materials are dielectric materials being well studied in hollow fiber research and the fabrication techniques and the fabrication parameters have been well established. Regarding the toxic risk in producing of PbS and CdS dielectric layers, both the coating process for SiO_2 and AgI are safe. And in our experiment R_2SiO is used to play the role as SiO_2 material and it can be formed in room temperature. No high temperature up to 200°C is necessary compared with the deposition process of SiO_2 when using per-hydro-polysilasane as precursor material. In addition to the inconvenience for fabrication in a high temperature, high temperature destroys the flexibility of hollow glass waveguides. Besides of the advantages mentioned, we also concluded that AgI and SiO_2 have good attachment with each other, so this kind of three-dielectric-layer hollow fiber will have strong durability and low-loss property. In this paper, the optimized dielectric film thickness is theoretically calculated and coating parameters for the films are discussed. The loss spectrum of three dielectric-layer hollow fiber is derived by using the ray optics model. The fabrication techniques of deposition three dielectric layers are experimentally discussed and the measured loss spectra during the fabrication process for a 35-cm long SiO_2/AgI/SiO_2/Ag hollow fiber were demonstrated.

2. Theoretical loss spectrum of multi-dielectric layer hollow fiber

The theoretical calculation for loss spectrum is based on the ray-optics theory [16]. This method was good to accurately predict the transmission property for hollow fiber. For a hollow fiber of length z, the transmitted power $P(z)$ is

$$P(z) = \int_0^{\theta_{max}} P_0(\theta) \exp\left[-\frac{1-R(\theta)}{2T\cot\theta} z \right] \sin\theta d\theta \qquad (1)$$

where $P_0(\theta)$ is the angular distribution of the incident beam, $R(\theta)$ is the power reflection coefficient, T is the inner radius of the hollow core and θ_{max} denotes the maximum launching angle. Theoretical result

of loss spectrum for the hollow fiber was obtained by calculating P(z) in a certain wavelength region. $R(\theta)$ can be calculated from the character matrix M, and matrix M for TE mode is calculated as equation 2, where $p = \sqrt{\frac{\varepsilon}{\mu}}\cos\theta$ and for TM mode p is substitute by $q = \sqrt{\frac{\mu}{\varepsilon}}\cos\theta$ [17]

$$M = \begin{bmatrix} m_{11} & m_{12} \\ m_{21} & m_{22} \end{bmatrix} = \begin{bmatrix} \cos(k_0 nz\cos\theta) & -\frac{i}{p}\sin(k_0 nz\cos\theta) \\ -ip\sin(k_0 nz\cos\theta) & \cos(k_0 nz\cos\theta) \end{bmatrix} \quad (2)$$

Then refractive coefficient can be derived by equation 3

$$r = \frac{(m_{11} + m_{12})p_l - (m_{21} + m_{22}p_l)}{(m_{11} + m_{12})p_l + (m_{21} + m_{22}p_l)} \quad (3)$$

Regarding multiple-layer calculation, matrix M_{total} can be calculated as followings,

$$M_{total}=M_1(z_1)M_2(z_2-z_1)M_n(z_N-z_{N-1}) \quad (4)$$

Where M_1 is the character matrix of the dielectric layer closest to the air core of hollow fibers, M_2 is that of the layer beneath the former layer, and M_n is that of the layer upon the metal layer. Then the equivalent $R(\theta)_{total}$ for multiple dielectric layers can be derived from the equivalent character matrix M_{total}. In the calculation, $R(\theta)$ is dependent on the refractive index of the dielectric film, material dispersion has a great influence on the shape and positions of low-loss valleys of the loss spectra. So in our calculation, material dispersion for AgI and SiO_2 is also taking into consideration in loss spectrum calculation [18].

The optimized dielectric layer thickness for SiO_2/AgI/SiO_2/Ag hollow fiber to deliver Er:YAG laser using our structure is also derived [5], the three dielectric layer from the air core to the metal layer should be 0.4μm, 0.43μm, and 0.7μm, respectively.

3. Fabrication Process

3.1. Inner-coating of Ag layer

The Ag layer is deposited on the inner wall of the capillary tube by liquid-phase chemistry method. The time for silver mirror reaction is set to 3 minutes. The thickness of silver layer is approximately 100 nm. The thickness of this layer can still be minored as long as the laser ray can be reflected back into the dielectric layer. A thinner silver film is normally of smaller surface roughness and thus the hollow fiber is of low-loss.

3.2. Inner-coating of SiO_2 layer

Per-hydro-polysilasane was used as a precursor in earlier research to deposit SiO_2 layer [13]. A high temperature up to 200°C is required, which damages the flexibility of hollow glass waveguides. And it also makes the method inappropriate for many other kinds of base tube materials, such as plastic tube. In our experiment we use OC300 [19], which is a semi-inorganic polymer based on the structural unit R_2SiO, to acts as the SiO_2 layer for it almost has the same optical property as SiO_2 in the visible and infrared regions. The advantage of this material is that it can be formed in the room temperature. The SiO_2 dielectric film is generated by the traditional sol-gel technique. The solution of a mixture of diluted

solution, hardener, and main solution with proportion 230:10:100 is pumped into the silver coated hollow fiber with a flow speed of 12 cm/min.

3.3. Inner-coating of AgI layer on SiO_2 film

The deposition of AgI layer on the SiO_2 film can be divided into two separated steps. The first step is to deposit the silver layer on the SiO_2 layer using the same liquid phase chemistry method mentioned in 3.1. However due to the existence of SiO_2 layer, the deposited thickness of silver layer is quite different from the thickness of silver layer deposited on the glass capillary tube. The rugged film layer will accelerate the sedimentation speed of Ag particles and lead to a thicker film layer. The second step is to transform the silver layer to silver iodide layer by iodination process. The thickness of AgI film thickness can be predicted using the formula published in our earlier work [14].

3.4. Fabrication for SiO_2 layer above AgI layer

This layer of SiO_2 film can be deposited on the AgI layer using the same techniques described in 3.2. And a curing treatment is also necessary after the sol-gel process to enhance the adhesion between SiO_2 layer and AgI layer.

4. Experiments results and discussion

4.1. Curing treatment in the deposition of SiO_2 layer

In our experiments, solution for sol-gel process is flown through the tube with the speed of 12 cm/min. To control the film thickness, we adjust the flowing speed. According to our experimental results, the empirical equation describing the relationship between film thickness and solution flow speed is

$$d = 220.8\sqrt{v} + 0.5685nm$$

when the mixing rate among diluted solution, hardener, and main solution are 230:10:100.

The SiO_2 layer formed in the room temperature can be well attached to the silver surface. But it proved to be destructible as long as another silver layer is deposit on it and iodination process is processed on the above silver layer. This may caused by the instability of the SiO_2 film. Before a solid film is formed, it needs quite a long time for the solvent in the solution to evaporate from the liquid-phase SiO_2 film. In order to speed up the evaporation speed for diluted solution, a curing treatment by heating up the hollow fiber to 80°C was followed after the sol-get process to form the SiO_2 layer. In the treatment, the hollow fiber was heated up to above 80°C for about 30 minutes, to accelerate the evaporation of solvent in the liquid-phase layer. By comparing the two loss spectra of the Ag/SiO_2 hollow fiber with and without the curing process, we note in fig. 1 that the position of interference peak has moved to lower wavelength and the loss has been reduced. It is clear that the absorption caused by the Si-O band in the wavelength region form 8 to 10 μm does not move.

Figure 2 shows the loss spectra of two $Ag/SiO_2/Ag$ hollow fibers. Silver layer 1 was deposited on a SiO_2 film that was not treated with the curing process, while silver layer 2 was treated. Silver layer 1 has much greater loss than that of silver layer 2, especially in short wavelength region. This means the curing treatment will contribute to a smoother Ag film according to the loss spectra for silver hollow fibers.

We can come to the conclusion that the curing process not only speed up the consolidate process of SiO_2 layer, but also leads to a thinner film and more uniformed SiO_2 film surface. And smoother Ag film above it can also be deposited.

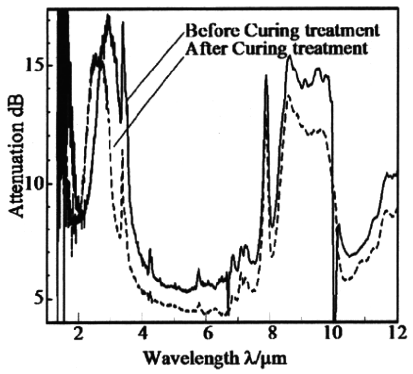

Fig. 1. Loss spectra for SiO_2/Ag hollow fiber before and after curing treatment

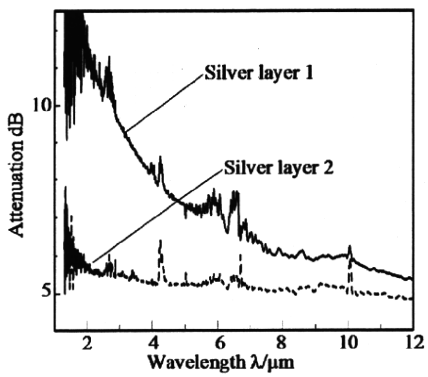

Fig. 2. Loss spectra of Ag/SiO_2/Ag hollow fibers with and without curing treatment for the SiO_2 layer

4.2. Thickness of silver layer on SiO_2 film

It is difficult to evaluate the thickness of Ag layer deposited on the SiO_2 film. We tried to measure the thickness by observing the cross-sectional image of the hollow fiber taken by the SEM. However, we could not determine the boundary between Ag and SiO_2 in the image, because both of them appear to be white in the photos as shown in figure 3 (a). We can see only one layer in the SEM picture.

Figure 3 (b) is the measured loss spectra of the same hollow fiber before and after silver layer being plated. The SiO_2/Ag hollow fiber has an obvious interference peak in the wavelength band of 2.5 μm due to thin SiO_2 film on the silver layer. After the deposition of silver layer, the loss spectrum is the same as a silver coated hollow fiber. It is shown that a silver layer is coated on the SiO_2 layer and the hollow fiber is of the structure of Ag/SiO_2/Ag.

Though chemical method was proposed [20] to measure the silver thickness by evaluating the remains of reaction products, this method is quiet complicated and time consuming. We proposed a method to calculate the silver thickness according to the AgI film thickness after all the Ag layer is transformed to AgI layer. From the reaction formula, the atom number of Ag is equal to the molecule number of AgI, and then the following equation can be derived:

$$\pi (r_1^2-r_2^2)\, \rho_{ag}\, L_{fiber}/M_{Ag} = \pi (r_1^2-r_3^2)\, \rho_{AgI} L_{fiber}/M_{AgI} \qquad (5)$$

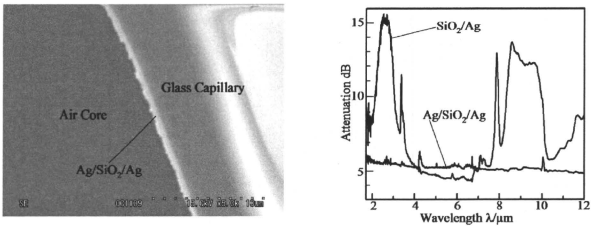

(a) (b)

Fig. 3 Cross-sectional image of $Ag/SiO_2/Ag$ hollow fiber(a) and measured loss spectrum SiO_2/Ag and $Ag/SiO_2/Ag$ hollow fiber(b)

As shown in fig. 4, the material from r_1 to r_2 is the origin Ag layer upon on SiO_2 layer, and r_1 to r_3 is the AgI layer after iodination. L_{fiber} is the length of hollow fiber.

In our structure, the radius r of hollow fiber is much greater than the film thickness d, and then equitation 5 can be transformed to equation 6

$$d_1\rho_{Ag}/M_{Ag} = d_2\rho_{AgI}/M_{AgI} \tag{6}$$

where the specific gravity is $\rho_{Ag}=10.5g/cm^3$ and $\rho_{AgI}=5.8g/cm^3$. The mole mass is $M_{Ag}=108$ and $M_{AgI}=235$, which means after the iodination process, the thickness of AgI film will approximately expand to 3.94 times of origin silver film thickness.

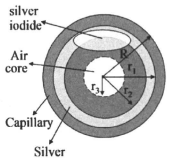

Fig. 4. Hollow fiber structure for AgI thickness evaluation

Table 1. Relationship between Silver layer thickness and silver mirror reaction time

Reaction time	Silver layer thickness on SiO_2 film	Silver layer thickness on capillary
3min40s	100~110	NA
4min	120~135	NA
4min30s	145~155	NA
5min	175~180	NA
5min30s	NA	120
12min	NA	260

Then using the calculated AgI film thickness data calculated from the hollow fiber fabricated by the method introduced in 3.2, the relationship between silver layer thickness on rugged SiO_2 layer and silver mirror reaction time is showed in table1. The silver thickness is much larger then the silver layer deposited on the capillary tube due to the roughness of SiO_2 film which accords with our earlier expectation.

4.3. Infiltration characteristic of SiO_2 film

In our earlier expectation, if the SiO_2 layer could resist the infiltration of iodination solution (cyclohexane as the solvent in our experiment), and the attachment ability of SiO_2 layer and AgI layer is good enough, we can use very long iodination time to ensure the whole silver layer on the SiO_2 film to be iodinated to AgI film. However from the experiment results, we found that despite the fact that in the introduction for R_2SiO film, it claims to be water repellence, the cyclohexane iodination solution can easily go through this SiO_2 layer and iodinated the silver layer on the capillary tube which is below the SiO_2 layer. Even the SiO_2 material after the curing treatment can't avoid the happening of this infiltration.

Figure 5 shows the SEM photo and the loss spectrum of the hollow fiber with the structure of SiO_2/AgI/Ag. The thickness of SiO_2 layer is 0.73 μm according to the spectrum of SiO_2/Ag hollow fiber. The dark layer in fig 5 (a) is the AgI film. It is formed by flowing iodination solution through the above SiO_2/Ag hollow fiber. The iodination time is 40 seconds and the concentration is 5g/L. The thickness of AgI layer is 0.26μm. From the spectrum curve fitting result, we can see that the calculated spectrum using SiO_2/AgI/Ag structure fits well with the measured loss spectrum.

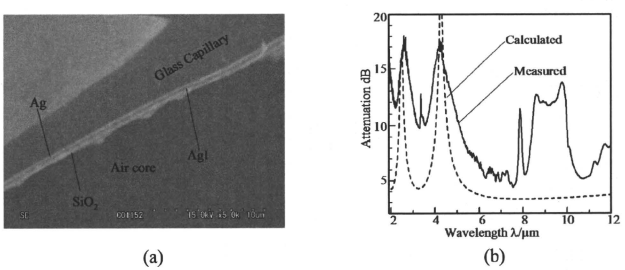

(a) (b)

Fig. 5. SEM photo for SiO_2/AgI/Ag hollow glass fiber (a), and measured loss spectrum for SiO_2/AgI/Ag hollow glass fiber (b), calculated loss spectrum was added for comparison

On considering the infiltration phenomenon of cyclohexane solution mentioned above, we should carefully control the iodination time to avoid the iodination of the silver layer under the SiO_2 layer when iodination the above Ag layer. On the other hand, it will simplify the iodination process for multiple layer structure by using the infiltration property. We can move the iodination process to the last step. And when all the silver layer and SiO_2 were orderly deposited, we can carry out the iodination process to convert all the silver layers between the SiO_2 layers into AgI layers. But again the iodination time should be carefully controlled in case the last silver layer on the capillary tube to be partly iodinated to AgI layer, and then the designed 2n+1 layer structure will be changed to the 2n+2 layer structure.

4.4. Results for SiO_2/AgI/SiO_2/Ag structure hollow fiber

In our experiment, we fabricated a three-dielectric-layer hollow fiber with the structure of SiO_2/AgI/SiO_2/Ag. The thicknesses for each dielectric layer from air core to the metal layer are 0.7 μm, 0.72 μm, 1.02 μm, respectively.

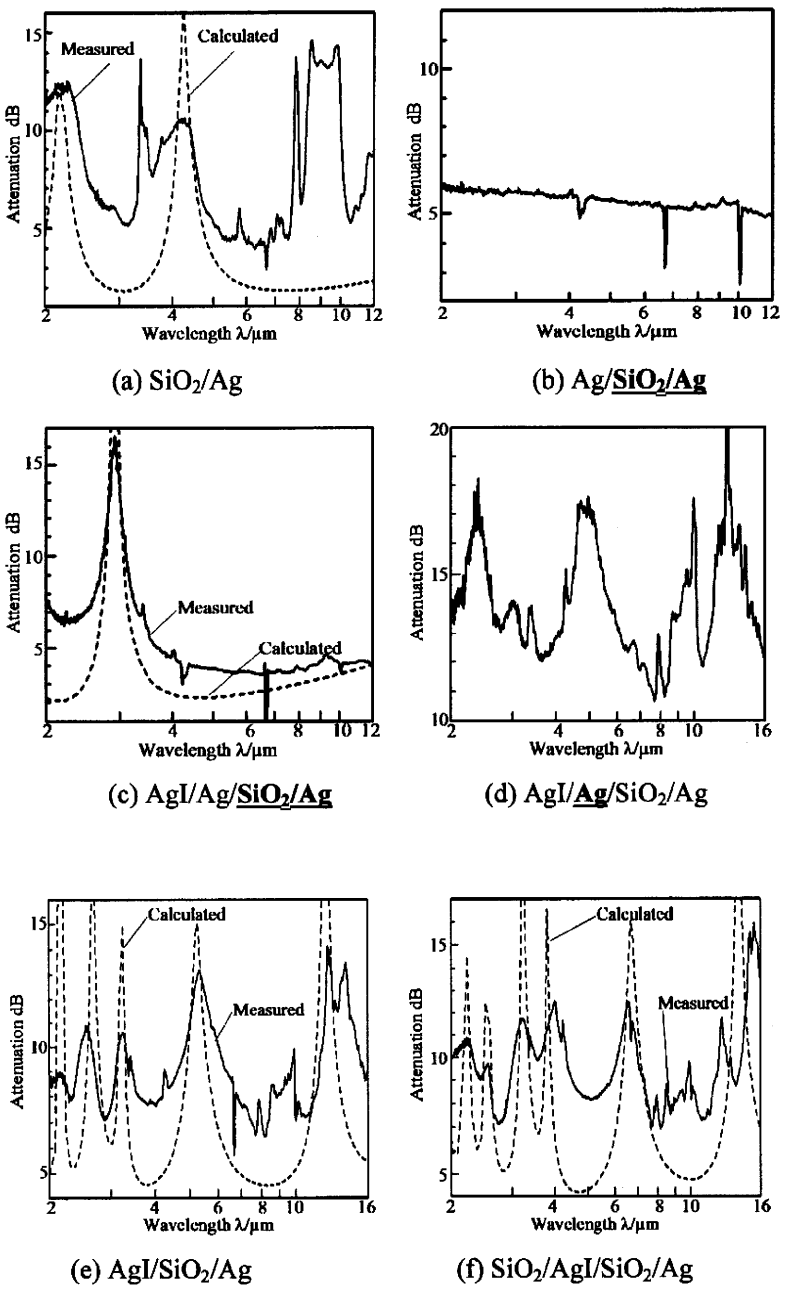

Fig. 6. Loss spectra of SiO_2/AgI/SiO_2/Ag hollow fiber during each step of fabrication

Using the fabrication process mentioned in Section 3, the silver and three layers were orderly deposited on the capillary tube. The measured and calculated loss spectra for every fabrication step are shown from Fig. 6 (a) to Fig. 6 (f).

Figure 6 (a) is the loss spectrum after SiO_2 layer is deposited and thickness of 1.02μm is calculated by curve fitting method. Figure 6 (b) is the loss spectrum for SiO_2/Ag hollow fiber, which is the same as an ordinary silver coated hollow fiber.

Figure 6 (c), 6 (d), and 6 (e) show the progress of the iodination procedure. Figure 6 (c) shows that the silver layer is partly iodinated by the cyclohexane iodination solution. The remained silver layer is thick enough that the fiber works as an AgI/Ag hollow fiber. With the progress of the iodination procedure, the remaining silver layer becomes thinner and thinner. Figure 6 (d) shows the loss spectrum of the hollow fiber when the remained silver layer is thinner than the skin depth. The absorption peaks of SiO_2 layer appear in the measured loss spectrum. And the measured loss spectrum shows large attenuation and noise, because of the very thin silver layer. When the iodination process continued, all the silver layer over the SiO_2 layer is turned into AgI, the loss of the spectrum decreases and fits the theoretical calculation result well again which is shown in figure 6 (e).

Then we coated the final SiO_2 film on the AgI layer. Figure 5(f) shows the loss spectrum for the SiO_2/AgI/SiO_2/Ag structure hollow fiber. According to the theoretical calculation, the dielectric film thickness from the metal layer to air core is 1.02μm, 0.72μm, 0.7μm respectively, the calculated loss spectrum fits well with the measured one in the mid-infrared regions. We note that the calculated curve in fig 6 (f) is the result for a 4-layer hollow fiber. The structure is SiO_2/AgI/SiO_2/AgI/Ag. This means that silver layer on the capillary was iodinated due to infiltration of the SiO_2 film. The film thickness of the AgI layer is 0.18 μm. Although it was not our intention to fabricate the 4-layer hollow fiber, it is difficult to accurately control the iodination time.

5. Summary

Transmission characteristics of infrared hollow fiber with multi- AgI and SiO_2 films are discussed. Three-dielectric-layer hollow fiber with SiO_2/AgI/SiO_2/Ag structure was fabricated for low-loss delivery of infrared laser light. Fabrication parameters are clarified for depositing AgI and SiO_2 films with the optimum thicknesses. Low-loss in the loss spectrum of SiO_2/AgI/SiO_2/Ag hollow fiber can be obtained at a target wavelength by optimizing the film thickness of each layer. Theoretical calculation for loss spectrum of SiO_2/AgI/SiO_2/Ag hollow fiber considering material dispersion of dielectric materials is conducted. Good agreement with the measured data is demonstrated.

6. Acknowledgements

This research is supported by the Scientific Research Foundation for the Returned Overseas Chinese Scholars, State Education Ministry and the National Nature Science Foundation of China (60608013), as well as by the Ministry of Education, Science, Sports and Culture of Japan through a Grant-in-Aid for Scientific Research (B) (20360164) and (B) (19760240) 2008 and Health and Labor Science Research Grants (H20-nano-young-010) 2008.

References

[1] George, R., and Harrington, J. A., "Infrared transmissive, hollow plastic waveguides with inner Ag–AgI coatings," Appl. Opt., 44(30), 6449-6455 (2005)

[2] Alaluf. M., Dror, J., Dahan, R., and Croitoru, N., "Plastic hollow fibers as a selective infrared radiation transmitting medium," J. Appl. Phys, 72(9), 3878-3883 (1992)

[3] Temelkuran, B., Hart, S. D., Benoit, G., Joannopoulos, J. D., and et al., "Wavelength-scalable hollow optical fibers with large photonic bandgaps for CO_2 laser transmission," Nature, 420(12), 650-653 (2002)

[4] Shi, Y. W., Ito, K., Ma, L. Yoshida, T., and et al., "Fabrication of polymer-coated silver hollow optical fiber with high performance," Appl. Opt., 45(26), 6736-6740 (2006)

[5] Miyagi, M., and Kawakami, S., "Design theory of dielectric-coated circular metallic waveguides for infrared transmission," J. Lightwave Technol. 2(2), 116-126 (1984)

[6] Ouyang, G. Xu, Y., and Yariv, A., "Comparative study of air-core and coaxial Bragg fibers: single-mode transmission and dispersion characteristics," Opt. Express, 9, 733-747 (2001)

[7] Fink, Y., Ripin, D. J., Fan, S., Chen, C., and et al., "Guiding optical light in air using an all-dielectric structure," J. Lightwave Technol., 17, 2039-2041 (1999)

[8] Matsuura, Y., Kasahara, R., Katagiri, T., and Miyagi, M., "Hollow infrared fibers fabricated by glass-drawing technique," Opt. Express, 10(12), 488-492 (2002)

[9] Miyagi, M., Hongo, A., Aizawa, Y., and Kawakami, S., "Fabrication of germanium-coated nickel hollow waveguides for infrared transmission," Appl. Phys. Lett, 43, 430-432 (1983)

[10] Matsuura, Y., and Harrington, J. A., "Infrared hollow glass waveguides fabricated by chemical vapor deposition," Opt. Lett, 20, 2078-2080 (1995)

[11] Croitoru, N., Dior, J., and Gannot, I., "Characterization of hollow fibers for the transmission of infrared radiation," Appl. Opt, 29, 1805-1809 (1990)

[12] Gopal, V., and Harrington, J. A., "Deposition and characterization of metal sulfide dielectric coatings for hollow glass waveguides," Opt. Express, 11(24), 3182-3187 (2003)

[13] Karagiri, T., Matsuura, Y., and Miyagi, M., "Metal-covered photonic bandgap multilayer for infrared hollow waveguide," Appl. Opt, 41(36), 7603-7606

[14] Sui, K. R., Shi, Y. W., Tang, X. L., Zhu, X. S. and et al., "Optical properties of AgI/Ag infrared hollow fiber in the visible wavelength region," Opt. Lett., 33(4), 318-320 (2008)

[15] Iwai, K., Miyagi, M., Shi, Y. W., Zhu X. S., and et al., "Infrared hollow fiber with a vitreous film as the dielectric inner coating layer," Opt. Lett., 32(23), 3420-3422 (2007)

[16] Matsuura, Y., Saito, M., and Miyagi, M., "Loss characteristics of circular hollow waveguides for incoherent infrared light," J. Opt. Soc. Am. A, 6(3), 423-427 (1989)

[17] Born, M., and Wolf, E., [Principles of Optics], Cambridge U. Press, Chap. 1(1999)

[18] Sui, K. R., Zhu, X. S., Tang, X. L., Iwai, K., and et al., "Method for evaluating material dispersion of dielectric film in the hollow fiber," Appl. Opt., 47(34), 6340-6344 (2008)

[19] Iwai, K., Shi, Y. W., Miyagi, M., Zhu, X. S., Matsuura, Y., "Hollow infrared fiber with an inorganic inner coating layer with high durability," Proc. SPIE 6433, p 64330L (2007)

[20] Matsuura, K., Matsuura, J. and Harrington, J. A., "Evaluation of gold, silver, and dielectric-coated hollow glass waveguides," Opt. Eng, 35(12), 3418-3421 (1996)

Simultaneous irradiation of Er:YAG and Ho:YAG lasers for efficient ablation of hard tissues

Tomonori Watanabe [1], Katsumasa Iwai [2], and Yuji Matsuura [1]

1) Tohoku University, Department of Electrical Communications Engineering, Sendai 980-8579, Japan
2) Sendai National College of Technology, Sendai 989-3128, Japan

Abstract

Hard tissues are irradiated with combined beam of Er:YAG and Ho:YAG lasers to achieve highly efficient ablation with lower laser power. We controlled the delay time between pulses of the two lasers and irradiated alumina ceramic balls that are used as hard tissue samples. By optimizing the delay time, the combined laser beam provides 40% higher perforation depth compared with the result with independent radiation of Er:YAG or Ho:YAG laser. The ablation mechanism are observed and investigated by using an ultra-high-speed camera and infrared thermography camera.

Keywords: Er:YAG laser, Ho:YAG laser, hard tissue ablation

1. Introduction

Since bio-tissues contain water that strongly absorbs infrared light, irradiation with infrared lasers gives a large effect on both of hard and soft tissues and therefore, it is applied to variety of medical applications [1]. In urological applications such as treatment of enlarged prostate and fragmentation of urinary calculi, Ho:YAG lasers with a wavelength of 2.1 μm is popularly used and the laser light is delivered by a common silica-glass fiberoptics incorporated in a thin endoscope to irradiate inside human body [2]. In dentistry applications, Er:YAG lasers with a 2.94-μm wavelength are commonly used because of the wavelength that coincides with a water absorption line which enables highly efficient ablation of hydroxyapatite that contains plenty of water. It is also reported that, with the Er:YAG lasers, more effective fragmentation of urinary calculi is possible [3] because the laser light is strongly absorbed with calcium oxalate and magnesium ammonium phosphate that are contained in urinary calculi [4]. Flexible silica-glass optical fibers cannot be used for delivery of Er:YAG lasers because of the absorption losses in relatively long wavelength region and to solve this problem, we have proposed and developed hollow optical fibers that deliver both of the Er:YAG and the Ho:YAG lasers with a high efficiency.

To rapidly break or perforate hard tissues, radiation of laser pulses with a high average power is necessary. However, this also generates heat in the vicinity of irradiated part that possibly causes damage or pain. In this paper, we investigate effects of simultaneous irradiation with Ho:YAG and Er:YAG lasers on hard tissues

Optical Fibers and Sensors for Medical Diagnostics and Treatment Applications IX, edited by Israel Gannot, Proc. of SPIE Vol. 7173, 71730R · © 2009 SPIE · CCC code: 1605-7422/09/$18 · doi: 10.1117/12.807910

such as calculi and teeth. We investigate ablation mechanisms of the lasers to achieve higher ablation effect for hard tissues.

2. Experiment and Discussion

We used an experimental setup shown in Fig. 1 to irradiate a hard tissue model with the two different lasers light. Ho:YAG (λ=2.1 μm) and Er:YAG (λ=2.94 μm) laser lights are combined by using a dichroic mirror and the laser beam is focused by a f=100 mm CaF_2 lens on the input end of a short hollow-fiber tip (100 mm in length) employed as a coupling optics. A hollow optical fiber with an inner diameter of 0.7 mm is butt-coupled to the short fiber that has the same diameter. The hollow fiber is coated with silver and cyclic-olefin polymer (COP) thin film on the inside and the thickness of COP is 0.3 μm so that the transmission losses for both of Er:YAG and Ho:YAG lasers are reduced by interference effect of the polymer film that acts as a reflection enhancement coating. The transmission losses of the hollow optical fiber used in the experiment are 1.0 dB for Ho:YAG and 0.5 dB for Er:YAG laser light.

The distal end of the hollow optical fiber is capped to keep the inside of fiber from vapor and debris of the ablated tissues. We used silica glass caps with a half ball shape. The focusing effect of the lens-shaped cap enables highly efficient ablation owing to the high energy intensity at the focal spot. The focal length of the cap is 1.0 mm from the end surface and the insertion loss is around 15%.

The emission timing and repetition rates of the pulses of the two lasers are controlled by an external trigger source and a delay line. To evaluate the ablation capabilities, we radiated lasers onto human teeth and alumina (Al_2O_3) ceramic balls used as a hard tissue model. We observed the ablation phenomenon by using an ultra-high-speed camera that has a capture speed of 50,000 frame/sec to investigate the ablation mechanism.

Firstly, we measured the depths and widths of ablated holes on alumina balls. We used alumina balls which are 4 to 6 mm in diameter and they had been soaked in water more than over night prior to the experiment.

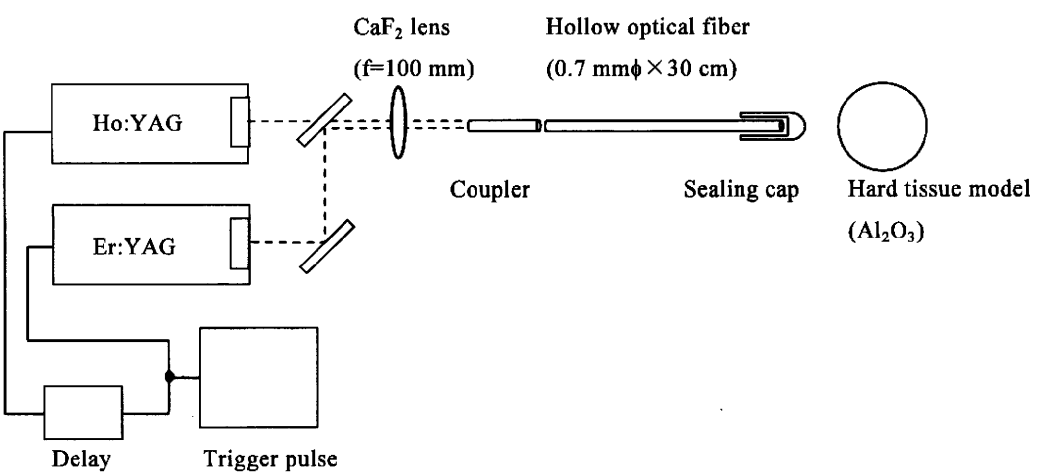

Fig. 1 Experimental setup with dual-wavelength laser

The pulse energies used in the experiment are 200 mJ and the pulse widths are 250 μs at the repetition rates of 3 Hz. The measured depths and widths as a function of pulse number are shown in Fig. 2 and cutting sections of ablated holes after 30 pulses are shown in Fig. 3.

It was found from the results in Fig. 2 that the widths are comparable for the both lasers and that, in contrast, the depths show clearly different appearances between the two lasers. When irradiated with the Ho:YAG, the depth saturated at large pulse numbers. This is because the energy density of the laser beam is getting lower than the ablation threshold of hard tissues when the beam spreads due to focusing effect of the lens cap. This happens in lower energy density for the Ho:YAG laser because of the lower absorption coefficient in water. For the Er:YAG, the depth increased linearly with the pulse shots because of the higher absorption coefficient in water.

Next we tested the ablation effect of the two lasers when they are simultaneously radiated. We change the delay time between the two lasers and observed the effect on ablation of ceramic balls. The pulse energies are 100 mJ for the both lasers and we compared the ablation depths with those made by the Er:YAG alone with a pulse

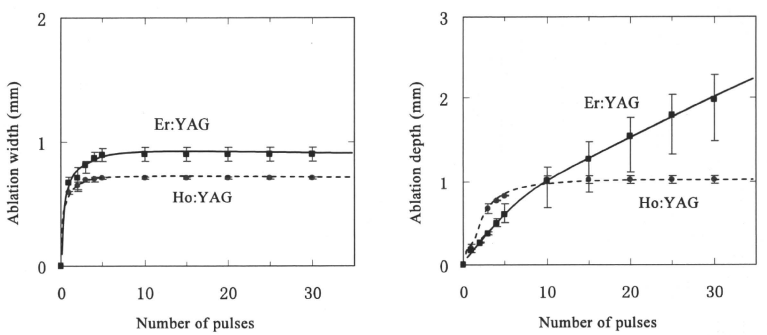

Fig. 2 Width and depth of ablated holes as a function of number of laser pulses

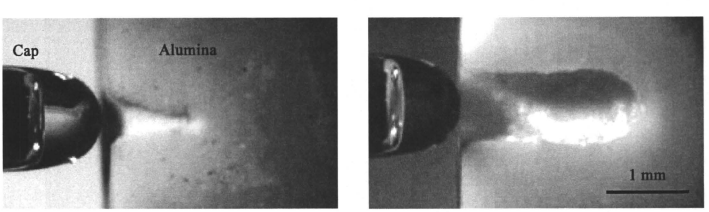

(a) Ho:YAG (b) Er:YAG

Fig. 3 Cutting sections of alumina balls after ablation of 30 pulses shot

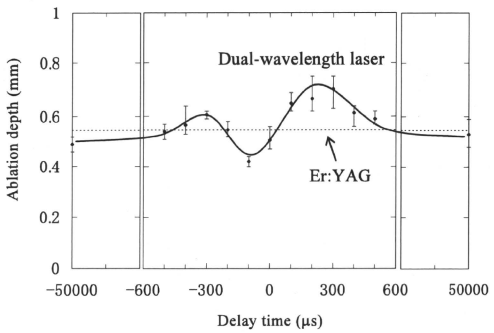

Fig. 4 Depths of ablated holes as a function of delay time

energy of 200 mJ. Figure 4 shows the depths of ablated holes as a function of delay time between the two lasers. The positive delay time means that we radiate the Ho:YAG before the Er:YAG. It is clear that the depths are highly dependent on the delay time and when irradiated with the delay time of $\pm$500 μs or smaller, depths drastically change with the delay. The largest depth is obtained at the delay time of 200-300 μs and obtained depth is 40% larger than that generated by the sole radiation of the Er:YAG laser.

To investigate the ablation mechanism of dual laser radiation, we observed the ablation phenomenon by using an ultra-high-speed camera. Alumina balls were irradiated with laser pulses and the moment of ablation at the surface was recorded at 50,000 frame/sec of capture speed. Figures 5 (a) and (b) show the ablation phenomenon with (a) Er:YAG and (b) Ho:YAG lasers alone and (c) is the moment of an Er:YAG pulse shot after

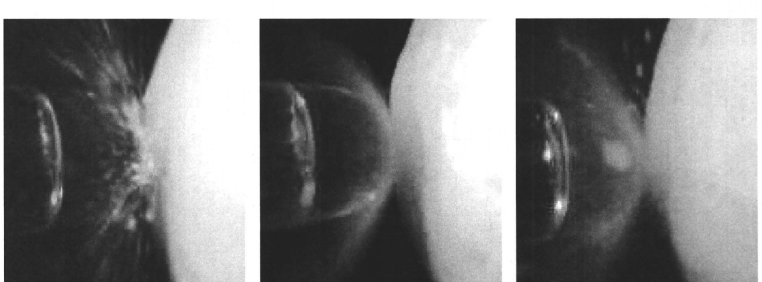

(a) Ho:YAG (b) Er:YAG (c) Ho:YAG and Er:YAG with a delay time of 200 μs

Fig. 5 Moment of ablation with Ho:YAG and Er:YAG lasers

a Ho:YAG with a delay time of 200 μs. When irradiated with Er:YAG laser light, powdery dust are scattered from the surface immediately after laser radiation. This is because the laser energy is absorbed in very surface of the ball. On the other hand, for the Ho:YAG laser, relatively large debris are sputtered. The laser beam penetrates into the ball and an explosive ablation occurred from the inside.

When an Er:YAG pulse is emitted after a Ho:YAG pulse (Fig. 5 (c)), large fragments were scattered. The Ho:YAG pulse that was radiated beforehand is absorbed and generates the heat. This causes decrease of absorption coefficient of water [5] and, as a result, Er:YAG laser beam can penetrates into the ball. In contrast, when a Ho:YAG pulse was shot after an Er:YAG, powdery dust were generated by Er:YAG and, after that, small debris were slightly sputtered from the surface. This is because the powdery dust scattered the most of the laser energy of delayed Ho:YAG pulse. As a result, the smallest depth was obtained in this case.

Next, we observed the heat generation during ablation of the alumina balls by using a thermographic camera. Figure 6 shows the thermal images of cutting sections of balls soon after laser radiation. When irradiated with Er:YAG laser, most of the pulse energy changed into the heat and stayed at the surface. In contrast, with the Ho:YAG laser, the energy penetrated deeper and therefore the induced heat diffused in a large area. This result comes from the difference of absorption coefficients and this is one of the reasons why the ablation with Ho:YAG occurred from the inside as shown in Fig. 5(a). At the optimum condition in Fig. 4 where the Er:YAG is emitted after Ho:YAG with a delay time of 200 μs, the heat was generated in deeper area before the Er:YAG pulse shot. This causes decrease of absorption coefficient of water and the Er:YAG laser beam penetrates deeper into the ball. Thermal lens effect may give an effect on deeper penetration as well.

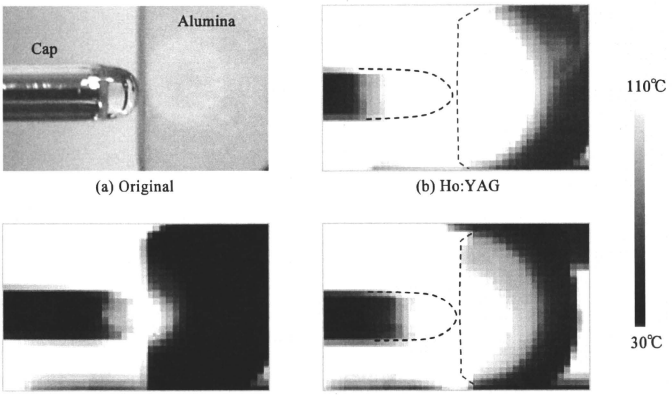

(a) Original (b) Ho:YAG

(c) Er:YAG (d) Ho:YAG and Er:YAG with a delay time of 200 μs

Fig. 6 Thermal images of cutting sections of balls after laser pulse